

From 3D static order to 2D dynamic correlations in the tetragonal double perovskite Sr_2CuWO_6

Oliver J. Burrows and Mark A. de Vries*
CSEC and School of Chemistry, University of Edinburgh, UK

Gøran J. Nilsen
*Institut Laue-Langevin, 72 Avenue des Martyrs, Grenoble, France and
ISIS, Rutherford Appleton Laboratory, Harwell Oxford, UK*

Emmanuelle Suard
Institut Laue-Langevin, 72 Avenue des Martyrs, Grenoble, France

Mark Telling and J. Ross Stewart
ISIS, Rutherford Appleton Laboratory, Harwell Oxford, UK

(Dated: February 15, 2016)

Sr_2CuWO_6 is a tetragonal ($I4/m$) double perovskite with diamagnetic W^{6+} ($5d^0$) and (Jahn-Teller-active) Cu^{2+} ($3d^9$) in a rocksalt-ordered arrangement on the B sites, modelling an anisotropic fcc-lattice antiferromagnet with $S = 1/2$. We have studied the magnetic structure, dynamics and thermodynamic properties of this material above and below the Néel-ordering transition at $T_N = 24$ K. Muon spin relaxation spectroscopy, neutron diffraction and neutron spectroscopy experiments show that the transition at T_N on heating is from static 3D type-2 antiferromagnetism to 2D dynamic correlations that remain detectable up to 100 K. Above T_N the muon relaxation is described by a compressed exponential decay, revealing a strong correlation between the spin fluctuation rate and the 2D correlation length. The low-temperature muon data and the entropy release around T_N as obtained from the heat capacity data point to small magnetic domains, probably of the order of 60 Å. We note that the material behaves more like a quasi-2D square lattice antiferromagnet than could be expected considering its structure only. A possible explanation might lie in the unusual strong spin-orbit-coupled magnetism of the W $5d$ levels, as the dominant exchange interaction is via the Cu-O-W-O-Cu pathway.

I. INTRODUCTION

Double perovskite Mott-Hubbard insulators have attracted much attention because of their interesting, often geometrically frustrated, magnetic topologies as well as the orbital degrees of freedom associated with high symmetry of the magnetic metal-ion environment¹. These features are exemplified by the B -site rocksalt-ordered double perovskites in which one of the B -sites contain orbitally-degenerate $4d$ or $5d$ transition metal ions with strong spin-orbit coupling (Mo^{5+} , Ru^{6+} , Re^{6+} , Os^{7+} and W^{5+}), which can be modelled as fcc lattices of antiferromagnetically-coupled spin-orbital moments with near-neighbour and next-nearest neighbour interactions². Against this backdrop the double perovskites Ba_2CuWO_6 and Sr_2CuWO_6 ³ provide model systems containing (perhaps by now reassuringly familiar) antiferromagnetically-coupled Cu^{2+} $J = S = 1/2$ spin moments, the W cations being in the nominally non-magnetic $6+$ state³⁻⁵. The Ba-analogue (Ba_2CuWO_6) has previously been shown to have a long-range ordered type-2 Néelground state with $T_N = 28$ K⁶, but because of the absence of any anomaly or field-cooled zero-field cooled splittings in the magnetic susceptibility Sr_2CuWO_6 was put forward as a potential quantum spin liquid⁵.

Sr_2CuWO_6 undergoes a Jahn-Teller distortion from cubic ($Fm\bar{3}m$) to tetragonal ($I4/mmm$) at 920°C, leading to an elongation of the c -axis ($c/a\sqrt{2} = 1.1$ for the body-centered tetragonal cell)⁴. At 670°C there is a further transition from $I4/mmm$ to $I4/m$ with a modest rotation of the octahedra around the c -axis, leading to the structure shown in Fig. 1. Subsequent studies on the magnetic properties of Sr_2CuWO_6 have focussed on the $I4/m$ phase. The magnetic Cu^{2+} $d_{x^2-y^2}$ orbital is aligned in the $a-b$ plane, causing some anisotropy between the in-plane and out-of-plane exchange constants. Figure 1 shows the four most important exchange interaction pathways; J_1 and J_3 are via Cu-O-O-Cu (90°) bonds in-plane and out-of plane respectively. J_2 and J_4 are via the Cu-O-W-O-Cu (180°) pathways in the $a-b$ plane and along the c -axis, respectively. As remarked earlier⁵, there is potential for geometrical frustration due to competing interactions along the different pathways. A recent μSR experiment has shown that there is long-range order below $T_N = 24$ K⁷, roughly an order of magnitude below the Weiss temperature. In the same study the exchange constants are estimated using DFT calculations combined with O K-edge X-ray absorption spectroscopy, yielding (strongest first): $J_2 = -7.47$ meV, $J_4 = -4.21$ meV, $J_1 = -1.2$ meV and $J_3 = -0.03$ meV⁷. While this is at first sight consistent with the crystallographic structure, the implied 3D antiferromagnetism is

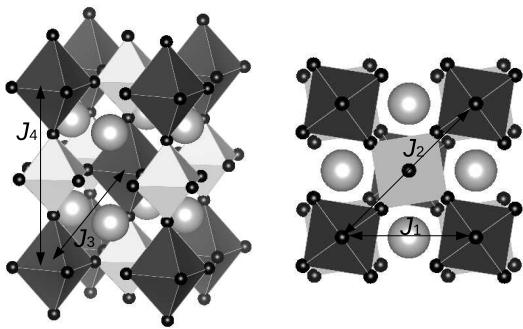


FIG. 1. The Sr_2CuWO_6 structure as seen from the side (c -axis pointing up) and from the top (along the c -axis). The arrows labelled $J_1 \dots J_4$ are the exchange pathways as described in the text. J_1 coincides with the a -axis ($= b$ -axis) and J_4 coincides with the c -axis.

difficult to reconcile with the magnetic properties which have previously been suggested to point to quasi-2D magnetism⁷.

The Mermin-Wagner theorem⁸ forbids magnetic ordering for $T > 0$ for any layered system where the interactions between $S = 1/2$ spins are strictly in the plane and short-ranged. In the case of the 2D square lattice of $S = 1/2$ spins with antiferromagnetic near-neighbour interactions the $T = 0$ ground state is expected to be long-range (Néel) ordered⁹ and in all known cases a 3D Néel-ordered state sets in at some finite temperature due to 3D interlayer interactions, which are often orders of magnitude smaller than the dominant in-plane exchange interactions¹⁰. Reduced ordered moments due to quantum fluctuations have been observed in physical realisations including copper formate tetradeuterate (CFTD)¹¹. The spin-wave dispersion exhibits distinctive non-classical features indicative of emergent $S = 1/2$ quasiparticle excitations¹². Furthermore, in many of these systems, including La_2CuO_4 ¹⁰, $\text{Sr}_2\text{CuO}_2\text{Cl}_2$ ¹³ and CFTD¹⁴, strong dynamic correlations have been found to persist far above the ordering temperature. Long-ranged 2D dynamic correlations in the $a - b$ planes, above T_N , have been hypothesised to explain the absence of any clear signatures of Néel ordering in the bulk magnetism in Sr_2CuWO_6 ⁷.

Notwithstanding all the work being carried out on Sr_2CuWO_6 , the magnetic ground state order is not yet known, nor is there any other than circumstantial evidence of dynamic correlations above the Néel temperature. This paper addresses both aspects with the aid of neutron powder diffraction, neutron spectroscopy, muon spectroscopy and heat capacity measurements. The experimental results confirm earlier suggestions that this material behaves like a quasi-2D antiferromagnet. An attempt is made to reconcile this behaviour with the apparently solidly 3D magnetic topology of this model system without invoking the concepts of geometrical frustration, which we argue do not play a role in Sr_2CuWO_6 .

II. EXPERIMENTAL DETAILS

Sr_2CuWO_6 was synthesised using standard solid state techniques. Stoichiometric quantities of SrCO_3 , CuO and WO_3 were ground in an agate mortar in air, before being pressed into a pellet and calcined at 900°C for two hours in air. The resulting compound was re-pelleted, then sintered at 1200°C (again in air) for 12 hours. The product was characterised using powder X-ray diffraction, and the sintering step was repeated until phase purity was achieved.

DC magnetic susceptibility measurements took place on a Quantum Design MPMS between 2 K and 400 K. Magnetization was measured as a function of temperature at a range of fields up to 7 T.

Heat capacity was measured on a Quantum Design PPMS, at temperatures between 2 and 300 K with 0.2 K steps between 20 and 30 K. A thin square pellet (1.5 mm by 1.5 mm, mass 9.5 mg) of sintered Sr_2CuWO_6 was affixed using Apiezon N grease (Dow Corning). The heat capacity of the grease was measured prior to the heat capacity of sample + grease, so that the heat capacity of the small sample could be extracted.

High-resolution neutron diffraction was carried out in the D2B beamline at the ILL on a 2 g sample in a cylindrical vanadium can. At 3.5 K the neutron diffraction data collected at wavelengths 1.594 Å (germanium monochromator (335) reflection) and 2.398 Å ((331) reflection) were refined together. At 50 K a wavelength of 2.398 Å was used, and at 298 K 1.594 Å. The uncollimated neutron beam was used with maximum slit openings.

The X-ray and neutron diffraction data were refined using the GSAS/EXPGUI^{15,16} software. Magnetic analysis of neutron diffraction was carried out using FULLPROF¹⁷ and the Bilbao Crystallographic Server.

Muon spin relaxation spectroscopy was carried out on the MuSR beamline at ISIS. Powdered sample was placed in a disc-shaped holder, and measured across a range of temperatures from 1.92 K to 199 K and in longitudinal fields from 0 G to 200 G. Measurements for data presented here were taken for 38.4 million positrons¹⁸ detected in each case. The polarization P_z is calculated from the asymmetry $A(t)$ using

$$P_z(t) = A(t)/A(t=0) \quad (1)$$

where $A(t) = B(t) - \alpha F(t)$ and α is a factor correcting for slight differences in efficiency of detecting forwards ($F(t)$) and backwards ($B(t)$) emitted positions. Above 27 K $A(t=0)$ was equated to the first data bin. Below 35 K it was clear from the sharp reduction of $A(t=0)$ compared to the higher temperature data that significant muon relaxation took place even within the “ $t=0$ ” bin and hence for $T < 35$ K a constant $A_T(t=0) = A_{35\text{K}}(t=0)$ was used.

Finally, inelastic neutron spectroscopy measurements were done on the MARI beamline at ISIS on a 60 g sample. The sample was placed in an aluminium foil envelope, which was rolled into annular configuration and

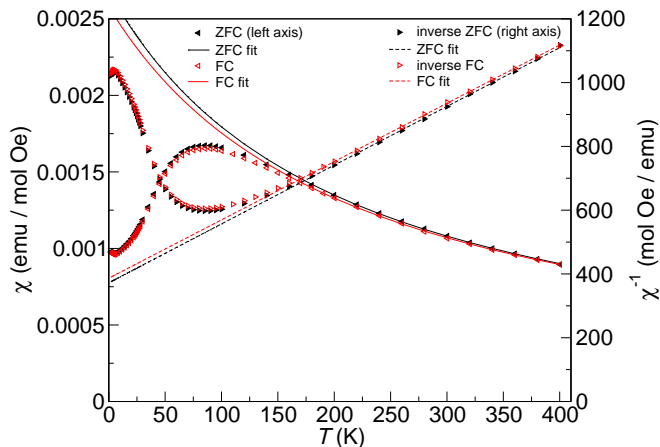


FIG. 2. Magnetic susceptibility (left axis, open symbols) and inverse susceptibility (right axis, filled symbols) of Sr_2CuWO_6 in zero-field-cooled (circles) and field-cooled (square) measurements, with fits to Curie-Weiss paramagnetism above 170 K.

placed in a 50 mm aluminium can. The incident energy was 30 meV, and measurements were taken at temperatures between 5 K and 200 K, using the thin-tail CCR.

III. RESULTS

A. Bulk measurements

Magnetometry measurements indicate that the high-temperature state, above 100 K, is Curie-Weiss paramagnetic. The Curie constant $C = 0.54 \pm 0.01 \text{ emu mol}^{-1} \text{ K}^{-1}$ corresponds to an effective moment $\mu_{\text{eff}} = 2.08 \mu_B$. The effective moment for Cu^{2+} is usually around $1.90 \mu_B$ and we do not have an explanation ready for the large effective moment observed here, except that perhaps there is some (minor) hybridisation between the Cu and W cations. This could cause an increased moment on the Cu (Cu^{3+} mixing in) as well as a small moment on the W, with W^{5+} mixing in. The Weiss temperature θ_{CW} is $-210 \pm 10 \text{ K}$ (Fig. 2). This differs from the Weiss constants of -116 K and -118 K previously reported by Vasala *et al.*¹⁹ and Iwanaga *et al.*²⁰, and is closer to the value of -230 K reported by Blasse³. There is a broad maximum just below 100 K that has been associated with the build-up of short-ranged correlations¹⁹ and then again a slight upturn below 10 K that could be due to paramagnetic impurities. No anomalies and no splitting between field-cooled and zero-field-cooled data are observed. This has previously led to speculation that Sr_2CuWO_6 has a 2D spin-liquid magnetic ground state¹⁹.

Our initial heat capacity data did not reveal any magnetic anomalies in the heat capacity (Fig. 3). Following the muon spin relaxation spectroscopy experiment by Vasala *et al.* revealing a transition at 24 K, more detailed measurements were done between 21 and 28 K.

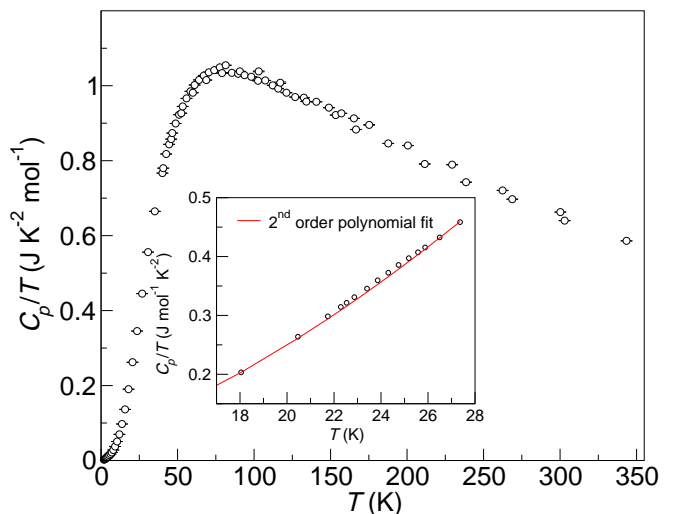


FIG. 3. Heat capacity of Sr_2CuWO_6 . Inset shows the region where a weak feature caused by the ordering seen in μSR is expected, compared to a background derived by fitting a 2nd-order polynomial to the C_p/T data surrounding the “peak”.

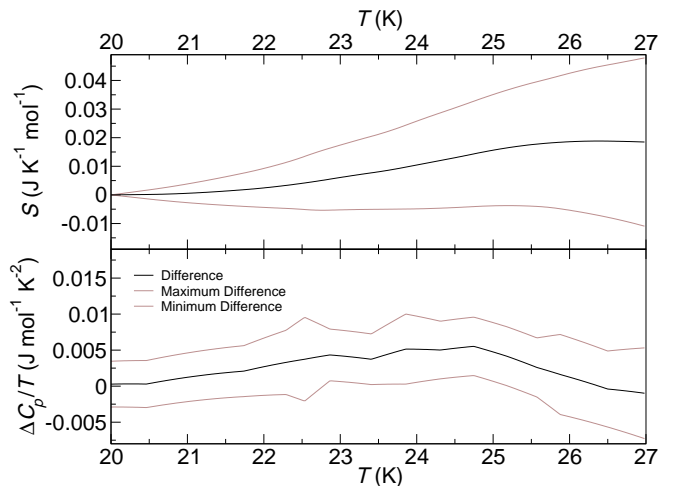


FIG. 4. Estimate of the magnetic entropy release at the transition (top) as a function of temperature (top) based on the difference with the fitted background heat capacity (bottom). The minimum and maximum difference give help to give an indication of the accuracy in the estimated entropy release. It is clear from this data that we can only provide an upper bound to the entropy release at the magnetic ordering transition.

These data revealed a very weak feature (Fig. 3(inset) and Fig. 4) and the entropy release at the transition (on heating through it from 20 to 26 K) is estimated at $0.3 \pm 0.2\%$ of the total magnetic entropy of $R \ln(2) = 5.76 \text{ J K}^{-1} \text{ mol}^{-1} (\text{Cu}^{2+})^{-1}$ (Figure 4).

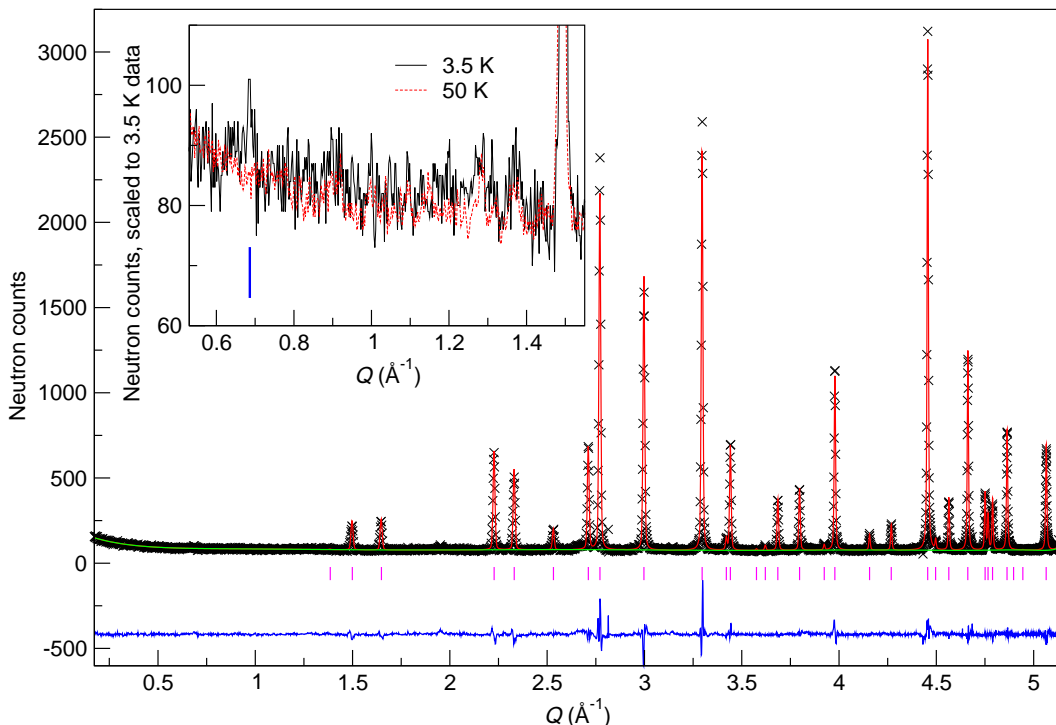


FIG. 5. Neutron diffraction pattern of Sr_2CuWO_6 at 3.5 K, neutron wavelength 2.398 Å. Inset: Comparison of 3.5 K (solid line) and 50 K (dashed line) neutron diffraction patterns, showing the magnetic peak at $Q = 0.69 \text{ \AA}^{-1}$. The blue vertical line indicates the position of the $(\frac{1}{2}, 0, \frac{1}{2})$ magnetic reflection.

B. Structural probes

The room-temperature neutron diffraction pattern of Sr_2CuWO_6 is shown in Fig. 5. The pattern was refined in the space group $I4/m$, as described in previous studies^{6,19}. Table I gives all details of the present refinement which is in good agreement with previous data. The data at 3.5 K show a very small additional peak at $Q = 0.68 \text{ \AA}^{-1}$ (Fig. 5(inset)). Comparison with a measurement at 50 K, as shown in the inset of Fig. 5, confirms that the reflection appearing at 0.68 \AA^{-1} is the only magnetic Bragg peak within the error bars of our measurements. The temperature dependence of the anisotropic displacement constants B for Cu and W is anomalous though the 50 K data should not be considered here as that data is with poorer statistics. That only the B of the Cu and W cations increases at low temperatures points to a magnetic effect, perhaps related to the small magnetic domains in the ordered state.

For comparison, the neutron diffraction pattern of Ba_2CuWO_6 in the magnetically-ordered state reveals two peaks⁶, the first like in Sr_2CuWO_6 at 0.68 \AA^{-1} , plus an additional reflection at 1.24 \AA^{-1} . The magnetic reflections in Ba_2CuWO_6 were indexed as $(\frac{1}{2}, \frac{1}{2}, \frac{1}{2})$ and $(\frac{1}{2}, \frac{1}{2}, \frac{3}{2})$ on a face-centred unit cell, corresponding to $(\frac{1}{2}, 0, \frac{1}{2})$ and $(\frac{1}{2}, 0, \frac{3}{2})$ in the body-centred tetragonal setting, respectively.

The magnetic structure implied by the $(\frac{1}{2}, 0, \frac{1}{2})$ peak

at 0.68 \AA^{-1} is the so-called type-2 structure, indexed by $k = (\frac{1}{2}, 0, \frac{1}{2})$ (magnetic space group $P_s\bar{1}$). This structure may be described as a series of antiferromagnetic planes stacked ferromagnetically along the b direction (Fig. 6). As for the Ba analogue, the ordered moment is very small, $\mu_o = 0.15 \pm 0.03 \mu_B$, and its orientation could not be determined reliably.

While Vasala *et al.* did not observe any magnetic Bragg peaks in their low-temperature neutron diffraction data, they did correctly predict the magnetic structure to be of type-2 with the aid of *ab-initio* calculations combined with X-ray absorption-spectroscopy data⁷.

C. Muon spin resonance

The previous μSR study revealed a sharp magnetic transition and yielded the field strength at the muon site as a function of temperature below $T_N = 24 \text{ K}$ ⁷. This transition is also observed in our data (Fig. 7) with a sharp drop in the $t = 0$ polarization between 25 and 20 K. The present data, collected at the ISIS facility (which is a high-intensity pulsed source) is complementary to the data by Vasala *et al.* taken at the Paul Scherrer Institute (PSI); the time resolution at MuSR at ISIS is lower, but the muon relaxation can be followed over much longer time scales (up to $16 \mu\text{s}$) due to the much higher number of muons implanted with each pulse/time frame. The muon source at PSI is a continuous source and therefore

TABLE I. Refinement results of Sr_2CuWO_6 at different temperatures. 3.5 K and 50 K data were refined from neutron diffraction data with neutrons of wavelength 2.398 Å; room temperature data were refined from neutron diffraction data with wavelength 1.594 Å.

T (K)	3.5	50	300
a (Å)	5.40965(4)	5.41065(3)	5.42902(3)
c (Å)	8.41368(7)	8.41397(6)	8.41614(8)
V (Å ³)	246.221(5)	246.320(4)	248.059(4)
Sr (0, 0.5, 0.25)			
B (Å ²)	0.11(4)	0.30(4)	0.44(2)
Cu			
B (Å ²)	0.33(7)	0.64(7)	0.13(4)
W			
B (Å ²)	0.42(9)	0.45(10)	0.07(6)
O1 ($x, y, 0$)			
x	0.2892(4)	0.2893(4)	0.2869(3)
y	0.2024(4)	0.2013(4)	0.2073(3)
B (Å ²)	0.21(3)	0.32(3)	0.38(2)
O2 (0, 0, z)			
z	0.2277(2)	0.2272(2)	0.2269(2)
B (Å ²)	0.02(5)	0.15(6)	0.73(3)
R_p (%)	7.09	4.24	4.97
R_{wp} (%)	8.96	5.75	6.80
R_{exp} (%)	5.53	1.64	2.50
χ^2	4.785	12.39	7.498

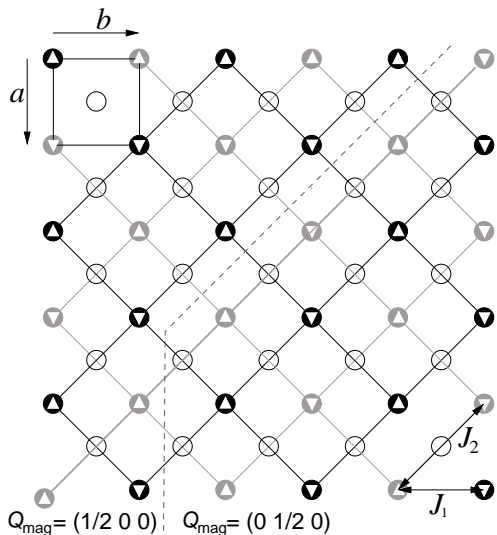


FIG. 6. A single layer with W^{6+} (open circles) and Cu^{2+} (circles with up/down triangle, i.e. spin inside) showing the spin configuration in a [001] $a - b$ plane. The same structure is also repeated in the [110] plane, which fully defines the type-2 antiferromagnetic structure. The dark and light lines represent the strong Cu-O-W-O-Cu J_2 exchange interactions, forming the two independent Cu^{2+} sublattices with dark and light circles. The dark sublattice is perfectly AF ordered. On the light (crystallographically equivalent) sublattice there is a phase shift causing a domain wall (broken line). At the domain wall on the light sublattice, the composite 2D magnetic wave vector k points along the a -axis (right) and at the domain boundary it rotates by 90° , to point along the b -axis (k').

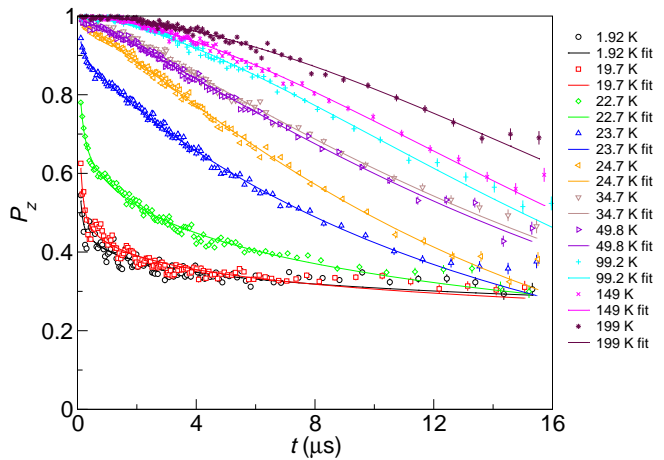


FIG. 7. MuSR on Sr_2CuWO_6 in zero field. Fits are to a linear combination of stretched exponential and fast Lorentzian decay (Equation 2).

better suited for measurements requiring a high time resolution.

Between 20 and 200 K the muon relaxation can be fitted with a (phenomenological) linear combination of Lorentzian and stretched exponential decays;

$$P_z = K_1 (e^{-\lambda t}) + K_2 (e^{-(\sigma t)^\beta}), \quad (2)$$

with the additional constraint that $K_1 + K_2 = 1$. λ and σ are the Lorentzian and stretched/compressed exponential relaxation factors respectively, and β is the stretching exponent - in the present case, with $\beta > 1$ the relaxation is *compressed* exponential, approaching $\beta \approx 1.8$ at high temperatures; $\beta = 2$ would equate Gaussian relaxation as expected for a paramagnet²¹. The results of the fits at temperatures between 2 K and 199 K are shown in Fig. 8. Down to 24.7 K, right above the ordering transition, the Lorentzian component remains close to zero and the relaxation is well modelled by the compressed exponential. As the system is cooled from 200 K there is a steady increase in σ and a gradual reduction in β , providing evidence of a gradual slow-down of the spin dynamics that starts at temperatures far above T_N .

Below $T_N = 24$ K a significant contribution from fast Lorentzian relaxation can be seen, and the stretching exponent β drops sharply to values below 1. Considering both the muon relaxation curves of Fig. 7 and the fit data of Fig. 8 it is clear that while the two components in Eqn. 2 accurately model two types of muon relaxation present in the sample above T_N , this is no longer the case below 20 K. In the 3D-ordered state strongly damped oscillations are observed, but in this case not with sufficient resolution to determine the ordered moment as a function of temperature, as was done by Vasala *et al.*⁷. The strong damping of the oscillations points to a wide distribution of local fields around the non-zero mean value. This is indicative of a fair amount of magnetic disorder,

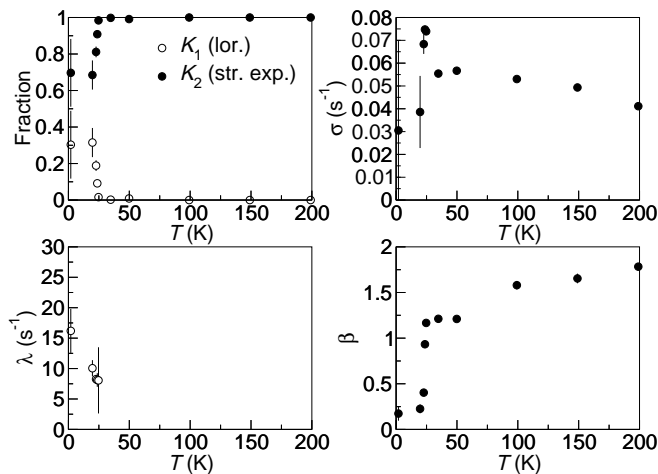


FIG. 8. Parameters to fits of muSR data for Sr_2CuWO_6 (see Fig. 7).

which may be due to the presence of many small magnetic domains, as we will see later. The relaxation to $1/3$ of the initial polarisation shows that one-third of the moments are aligned parallel or antiparallel with the initial muon polarisation, as expected for static moments in a powder sample with no preferential crystallographic and therefore magnetic orientation.

D. Inelastic neutron scattering

Inelastic neutron scattering measurements were carried out to characterise the dynamic magnetic correlations as a function of temperature. 30 meV neutrons were used ($\lambda = 1.65 \text{ \AA}$) and the neutron spectrum taken at 5 K is shown in Fig. 9. The two bands below 1.5 \AA^{-1} , rising up to approximately 14 meV, are of magnetic origin – no structural reflections occur at these wave numbers. We focus in particular on the part of the magnetic dispersion rising up from approximately $Q = 0.68 \text{ \AA}^{-1}$, where the $(\frac{1}{2}, 0, \frac{1}{2})$ reflection is located at the elastic line. In Fig. 10 the inelastic scattering in this area is shown as a function of temperature.

The energy window for neutrons at these short wave numbers is rather narrow regardless of the energy of the incident neutrons, but with 30 meV neutrons a significant section of the magnetic spin-wave dispersion and dynamic magnetic correlations can still be observed. The zero-energy-transfer origin of the dispersion, and center of mass, appears to be at about 0.62 \AA^{-1} , somewhat below the elastic magnetic reflection at 0.68 \AA^{-1} . Figure 11 shows the neutron scattering intensity integrated over energies from 4 to 6 meV and corrected for the magnetic form factor, showing the same mismatch. The reason for the mismatch is that the dispersion observed here does *not* correspond to the 3D spin-waves in the *ordered* phase. The energy scale of the 3D ordering is up to $\sim 2 \text{ meV}$ and the signal up to that energy is swamped by

the elastic line and hence is invisible here. The dispersion observed here corresponds to 2D dynamic antiferromagnetic correlations – the energy scale of 14 meV ($\approx 162 \text{ K}$) is of the order of the in-plane magnetic exchange interactions. It is then not surprising that the dispersion curves remain practically unchanged on heating above the ordering transition, with strong correlations visible even at 50 K and still just about visible at 100 K.

The energy-integrated scattering shown in Fig. 11 exhibits a peak shape that is characteristic of 2D correlations in a powder sample, as described by Warren^{22,23};

$$I = \frac{C \left(1 - 2 \left(\frac{\lambda Q}{4\pi} \right)^2 + 2 \left(\frac{\lambda Q}{4\pi} \right)^4 \right) \sqrt{\frac{\xi}{\lambda\sqrt{\pi}}} \times \int_0^{20} F(a) dx}{\left(\frac{\lambda Q}{4\pi} \right)^{\frac{3}{2}}} + K \quad (3)$$

where

$$F(a) = e^{-(x^2 - a)^2} \quad (4)$$

and

$$a = \frac{\xi\sqrt{\pi}(Q - Q_0)}{2\pi} \quad (5)$$

and $\lambda = 1.65 \text{ \AA}$ is the neutron wavelength. The wave vector obtained from the fit $Q_0 = 0.592 \pm 0.002 \text{ \AA}^{-1}$ corresponds to the in-plane $(\frac{1}{2}, 0, 0)$ antiferromagnetic wave vector. Strictly speaking, the Warren function (Eq. 3) describes only the *elastic* scattering from short-ranged 2D correlations. In the present case we integrate over a small range of (relatively-low) inelastic energies as is in practice inevitable in diffuse neutron scattering. Here it is justified by the energy independence of the neutron-scattering cross section within and, where visible, outside the interval of energies included in the integral. Hence this data confirms that the magnetic correlations above T_N are 2D (in the $a-b$ planes), and persist, if weakly, up to 100 K. The fits yield a lower limit to the correlation length ξ as a function of temperature, shown in Fig. 12.

IV. DISCUSSION

The presence of 2D dynamic antiferromagnetic correlations above T_N and up to $\sim 100 \text{ K}$, as observed in the neutron spectra of Figs. 10 and 11, explains the absence of an anomaly at T_N in the magnetic susceptibility. We can conclude that below the broad maximum in the magnetic susceptibility data (Fig. 2) at 100 K antiferromagnetic spin correlations start to grow as the temperature is lowered, while not far above 100 K Curie-Weiss paramagnetism sets in. The μSR data show that there is a gradual slowing down of spin fluctuations with increasing 2D spatial correlations, but that the spins remain dynamic until cooled below T_N .

These observations are also consistent with the very small peak that can just be discerned in the heat capacity data between 20 and 26 K, peaking at $\sim 24 \text{ K}$. The (2D)

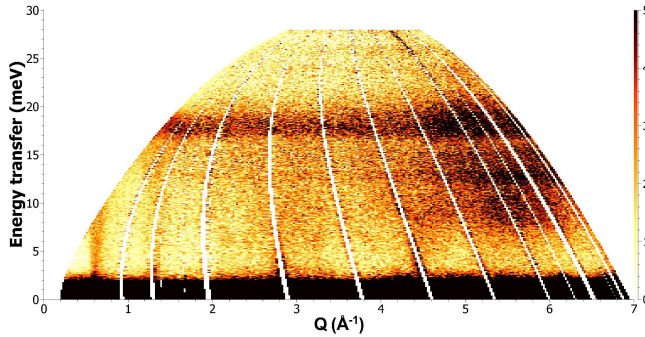


FIG. 9. Full inelastic neutron scattering spectrum of Sr_2CuWO_6 at 5 K.

magnetic wave vector in the 2D layers is $(\frac{1}{2}, 0)$ and this leads to three distinct ways an ordered 2D layer can be stacked on the preceding one along the c -axis: shifted by $1/2$ a phase along the magnetic k -vector, and rotated by 90° around the c -axis. The entropy associated with the 2D- to 3D-ordering transition can then be calculated as follows: the total number of distinct configurations of l 2D ordered layers $\Omega(l) = 3^{l-1}$. Hence the entropy of the 2D- to 3D-ordering transition as a function of l is given by

$$S_{2\text{D}-3\text{D}}(l) = \ln[\Omega(l)] = \ln(3^{l-1}) = (l-1) \ln(3) \propto n^{\frac{1}{3}} \ln(3), \quad (6)$$

where n is the total number of magnetic $S = 1/2$ spins in a sample grain or in the coherent volume. Note that we see from the approximate equation at the right-most side that this entropy is subextensive. If we assume that the coherent volume below the transition contains an equal number of spins along each crystallographic axis then the total magnetic entropy of that volume can be written as

$$S_{\text{magnetic}}(l) = l^3 \ln(2) \quad (7)$$

and the ratio

$$S_{2\text{D}-3\text{D}}(l)/S_{\text{magnetic}}(l) = \frac{l-1}{l^3} \frac{\ln(3)}{\ln(2)} \quad (8)$$

The experimentally-obtained ratio of 0.003 (0.3%) (an upper limit) yields $l = 15$, which translates to an upper limit for the correlation length of 63 \AA along the c -axis and 81 \AA in the $a-b$ plane. This is reassuringly close to the correlation length in the $a-b$ plane just above the transition (55 \AA), as obtained from the Warren fits. It is also consistent with the fast muon relaxation to $P_z = 1/3$ below T_N , which points to small coherent antiferromagnetic domains in the low-temperature 3D-ordered phase. Given the degeneracy intrinsic to the type-2 magnetic ordering discussed earlier, these are likely to be domains, with the in-plane component of the magnetic k vector

variably aligned along the crystallographically-equivalent a - and b -axes.

The available data are fully consistent and readily explained by the presence of strong 2D correlations persisting above T_N , in what could be described as a “2D thermal spin liquid” phase at intermediate temperatures. While this is in line with earlier proposals⁷ it is not clear how this phase arises if the computational exchange constants⁷ are correct – in particular if J_4 is indeed as strong as -4.21 meV (49 K), 56% of the dominant J_2 exchange. This would not be a quasi-2D system and could be expected to show 3D Néel ordering around at least 50 K. Note that the two interpenetrating 3D sublattices arising from the J_2 and J_4 bonds only (Fig. 6) are not by themselves frustrated. When they order fully antiferromagnetically, each with a wave vector $(\frac{1}{2}, \frac{1}{2}, \frac{1}{2})$, there is a two-fold degeneracy arising from the relative phase of the two sublattices. Both degenerate states are type-2 antiferromagnetic, with the in-plane antiferromagnetic phase vector aligned along the a or the b axis. This degeneracy is not lifted by inclusion of the much weaker J_1 and J_3 because for each J_1 edge with antiferromagnetically aligned spins at the vertices there is a J_1 edge with ferromagnetically aligned spins.

Hence, the observed type-2 antiferromagnetism is consistent with the predicted exchange constants, but the dynamic correlations in the 2D thermal spin liquid state above T_N are not. In the archetypical quasi-2D antiferromagnet La_2CuO_4 the ratio between the interplane exchange constant and the main in-plane exchange interaction $J_\perp/J_1 = 10^{-5}$. This is hugely different from the ratio between the predicted J_4 and J_2 for Sr_2CuWO_6 , considering that the ratio of the Néel temperature T_N over J_1 in La_2CuO_4 ; $300 \text{ K} / 1345 \text{ K} = 0.22$, is only slightly less than T_N over J_2 in Sr_2CuWO_6 . Furthermore, the short-ranged correlations evident above T_N in Sr_2CuWO_6 are 2D and strongly reminiscent of the magnetism in La_2CuO_4 above 300 K. Hence, it is very unlikely that the theoretically-predicted value for $J_4 = -4.21 \text{ meV}$ is correct.

One possible explanation for the computational overestimate lies in the role of the W $5d^1$ orbital. The W cations are part of the J_2 and J_4 interaction pathways and XAS by Vasala *et al.*⁷ indicates that there is some overlap between the Cu $3d - \text{O } 2p$ bands and the W $5d - \text{O } 2p$ bands. It may then be of relevance that the magnetism of W $5d^1$ electrons in an octahedral crystal field is described by a Kugel-Khomski Hamiltonian in the limit of strong spin-orbit coupling, as described in detail by Gang-Chen *et al.*¹. This gives rise to a magnetic Hamiltonian in which the exchange pathway itself depends on the orientation of the magnetic (spin-orbital) moments. Combined with the solid orbital ordering of the magnetic $\text{Cu}^{2+} d_{x^2-y^2}$ orbital in the $a-b$ plane, perhaps the strongly spin-orbit-coupled magnetism of the W cation causes a much greater difference between J_2 and J_4 interactions. This is something that might be worth exploring in further detail. Further neutron spectroscopy experiments, from

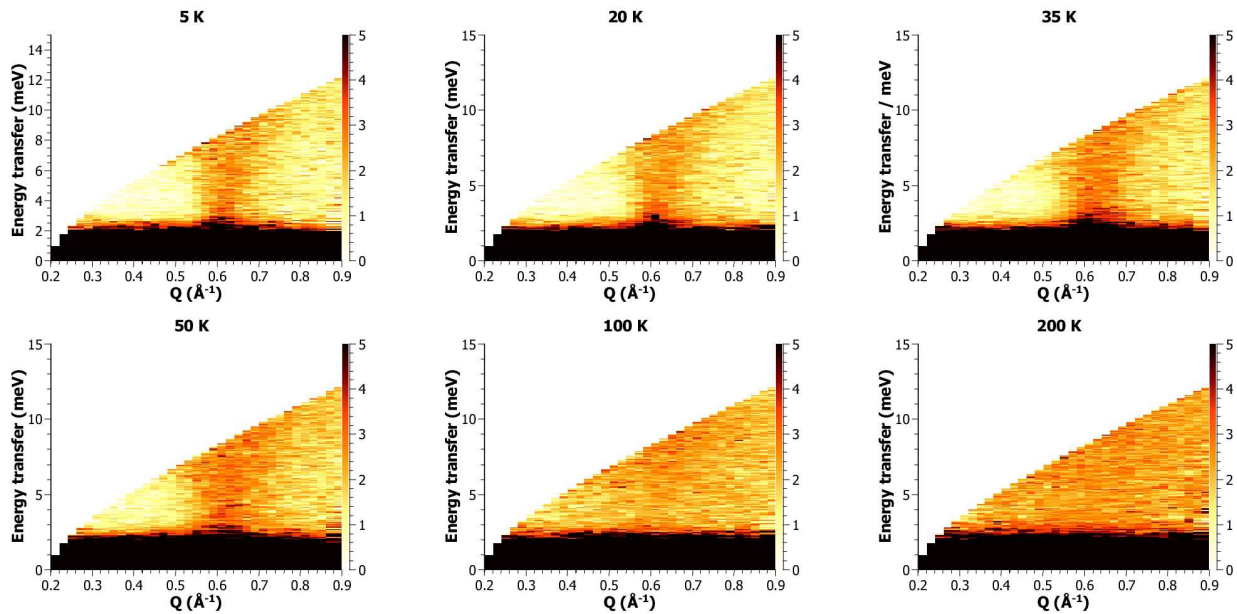


FIG. 10. Inelastic neutron scattering spectrum of Sr_2CuWO_6 at a range of temperatures, showing strong scattering at $Q = 0.63\text{\AA}^{-1}$ below 100 K.

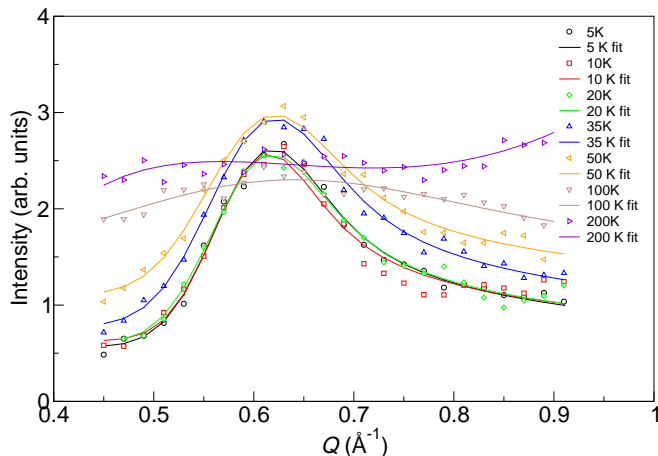


FIG. 11. Warren function (Equation 3) fit to inelastic peak below 100 K, integrated between 4 meV and 6 meV.

which the exchange constants could be determined via spin-wave modelling, would also be beneficial but probably only if done using large single crystals which are presently not available.

With regards to the muon relaxation in the thermal spin liquid regime, it is worth noting that compressed exponential relaxation has been observed in other spin liquid phases, for example in $\text{SrCr}_8\text{Ga}_4\text{O}_{19}$ (SCGO)²⁴, herbertsmithite ($\text{ZnCu}_3(\text{OH})_6\text{Cl}_2$)²⁵ and the double perovskite Ba_2YMoO_6 ²⁶. In SCGO the compressed exponential approaches Gaussian ($\beta = 2$) as the temperature is lowered and it is thought to arise from a dynamical and heterogeneous ground state with a mixture of unpaired spins and spins paired into spin-singlet dimers²⁴,

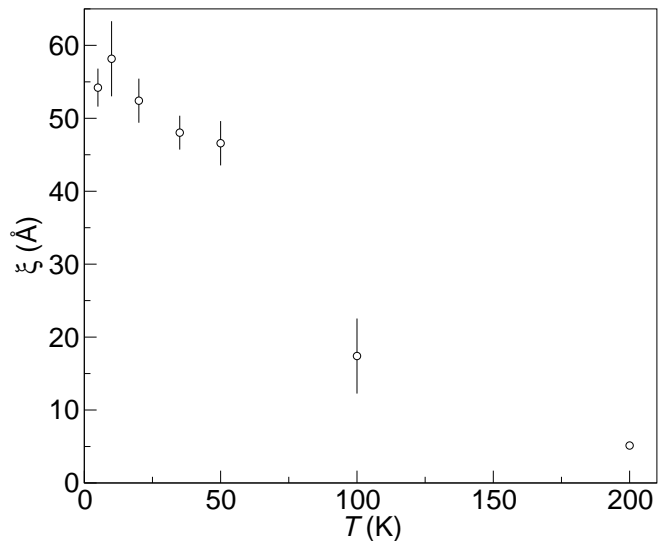


FIG. 12. Change in correlation length in Warren function with temperature.

so that any particular muon environment fluctuates between magnetic and non-magnetic at a time scale shorter than the muon lifetime. This inevitably gives rise to a lifetime faster than that observed for the other examples and in Sr_2CuWO_6 there is no evidence of spin-singlet dimers, as they would be manifest in neutron spectroscopy data as near-neighbour antiferromagnetic correlations only. This also rules out any fundamental similarity with the spin liquid states in herbertsmithite and Ba_2YMoO_6 as both states are thought to be dominated by near-neighbour spin-singlet²⁷ and spin-orbital

singlet dimers²⁶, respectively. In Ba₂YMoO₆ the compressed exponential muon relaxation is the result of two distinct muon environments: those adjacent to unpaired (dangling) fluctuating spins and those sitting elsewhere in the material, surrounded by non-magnetic spin-orbital singlet pairs. Hence there is a rather large variety of scenarios that give rise to compressed exponential relaxation and they have to be considered case by case. No further parallels can be drawn between the case of Sr₂CuWO₆ and the others.

V. CONCLUSIONS

Below 24 K the quasi-2D square lattice antiferromagnet Sr₂CuWO₆ freezes into a 3D-ordered Néel state with k-vector $(\frac{1}{2}, 0, \frac{1}{2})$, pointing to type-2 antiferromagnetic order (magnetic space group $P_5\bar{1}$) as predicted previously based on X-ray absorption spectroscopy combined with computational studies⁷. As often for quasi-2D antiferromagnets with $S = 1/2$, neutron spectroscopy shows that

dynamic 2D correlations are detectable far above T_N ; in this case up to ~ 100 K, a temperature that is comparable to the energy scale of the main exchange interaction estimated at $J_2 \sim -90$ K and coinciding with the maximum in the magnetic susceptibility. Furthermore, μ SR shows a pronounced slowing down taking place well before T_N is reached on cooling.

The pronounced 2D character of the magnetism is however surprising in the light of the exchange constants one might expect considering the structure of Sr₂CuWO₆. Perhaps the spin-orbit coupling in the $5d^1$ band of the W cations on the dominant exchange interaction pathway, not taken into account in the reported calculations⁷, can explain the large difference between in-plane and out-of-plane exchange interactions implied by the above observations.

ACKNOWLEDGMENTS

The authors thank EPSRC for Ph.D. student funding (OB), and the STFC and ILL for beam time.

-
- * m.a.devries@ed.ac.uk
- ¹ G. Chen, R. Pereira, and L. Balents, *Physical Review B* **82**, 174440 (2010).
 - ² W. Witzak-Krempa, G. Chen, Y. B. Kim, and L. Balents, arXiv:1305.2193 (2013).
 - ³ G. Blasse, *Journal of Inorganic and Nuclear Chemistry* **27**, 993 (1965).
 - ⁴ M. Gateshki, J. M. Igartua, and E. Hernández-Bocanegra, *Journal of Physics: Condensed Matter* **15**, 6199 (2003).
 - ⁵ S. Vasala, J. Cheng, H. Yamauchi, J. B. Goodenough, and M. Karppinen, *Chemistry of Materials* **24**, 2764–2774 (2012).
 - ⁶ Y. Todate, W. Higemoto, K. Nishiyama, and K. Hirota, *Journal of Physics and Chemistry of Solids* **68**, 2107 (2007).
 - ⁷ S. Vasala, H. Saadaoui, E. Morenzoni, O. Chmaissem, T. Chan, J. Chen, Y. Hsu, H. Yamauchi, and M. Karppinen, *Physical Review B* **89**, 134419 (2014).
 - ⁸ N. D. Mermin and H. Wagner, *Physical Review Letters* **17**, 1133 (1966).
 - ⁹ E. Manousakis, *Rev. Mod. Phys.* **63**, 1 (1991).
 - ¹⁰ B. Keimer, N. Belk, R. J. Birgeneau, A. Casanholo, C. Y. Chen, M. Greven, M. A. Kastner, A. Aharony, Y. Endoh, R. W. Erwin, and G. Shirane, *Phys. Rev. B* **46**, 14034 (1992).
 - ¹¹ H. M. Rønnow, D. F. McMorrow, R. Coldea, A. Harrison, I. D. Youngson, T. G. Perring, G. Aeppli, O. Syljuåsen, K. Lefmann, and C. Rischel, *Phys. Rev. Lett.* **87**, 037202 (2001).
 - ¹² B. Dalla Piazza, M. Mourigal, N. B. Christensen, G. J. Nilsen, P. Tregenna-Piggott, T. G. Perring, M. Enderle, D. F. McMorrow, D. A. Ivanov, and H. M. Rønnow, *Nature Physics* **11**, 62 (2015).
 - ¹³ M. Greven, R. J. Birgeneau, Y. Endoh, M. A. Kastner, M. Matsuda, and G. Shirane, *Zeitschrift für Physik B Condensed Matter* **96**, 465 (1995).
 - ¹⁴ H. M. Rønnow, D. F. McMorrow, and A. Harrison, *Phys. Rev. Lett.* **82**, 3152 (1999).
 - ¹⁵ A. C. Larson and R. B. Von Dreele, *General Structure Analysis System (GSAS)*, Tech. Rep. LAUR 86-748 (Los Alamos National Laboratory, 1994).
 - ¹⁶ L. Toby, *Journal of Applied Crystallography* **34**, 210 (2001).
 - ¹⁷ J. Rodríguez-Carvajal, *Physica B: Condensed Matter* **192**, 55 (1993).
 - ¹⁸ Positrons are emitted as a muon decay product. The direction of their emission is preferentially along the direction the muon spin pointed in at the time that muon decayed.
 - ¹⁹ S. Vasala, J. Cheng, H. Yamauchi, J. B. Goodenough, and M. Karppinen, *Chemistry of Materials* **24**, 2764 (2012).
 - ²⁰ D. Iwanaga, Y. Inaguma, and M. Itoh, *Journal of Solid State Chemistry* **147**, 291 (1999).
 - ²¹ T. Aharen, J. E. Greedan, F. Ning, T. Imai, V. Michaelis, S. Kroeker, H. Zhou, C. R. Wiebe, and L. M. D. Cran-swick, *Phys. Rev. B* **80**, 134423 (2009).
 - ²² B. E. Warren, *Physical Review* **59**, 693–698 (1941).
 - ²³ A. S. Wills, N. P. Raju, C. Morin, and J. E. Greedan, *Chemistry of Materials* **11**, 1936 (1999).
 - ²⁴ Y. J. Uemura, A. Keren, K. Kojima, L. P. Le, G. M. Luke, W. D. Wu, Y. Ajiro, T. Asano, Y. Kuriyama, M. Mekata, H. Kikuchi, and K. Kakurai, *Phys. Rev. Lett.* **73**, 3306 (1994).
 - ²⁵ P. Mendels, F. Bert, M. A. de Vries, A. Olariu, A. Harrison, F. Duc, J. C. Trombe, J. S. Lord, A. Amato, and C. Baines, *Physical Review Letters* **98**, 077204 (2007).
 - ²⁶ M. A. de Vries, J. O. Piatek, M. Misk, J. S. Lord, H. M. Rønnow, and J. G. Bos, *New Journal of Physics* **15**, 043024 (2013).
 - ²⁷ M. A. de Vries, J. R. Stewart, P. P. Deen, J. O. Piatek, G. J. Nilsen, H. M. Rønnow, and A. Harrison, *Physical Review Letters* **103**, 237201 (2009).